Atmospheric Environment 209 (2019) 125–135

Contents lists available at ScienceDirect

Atmospheric Environment

journal homepage: www.elsevier.com/locate/atmosenv

Modelling microbial kinetics and thermodynamic processes for quantifying soil CO_2 emission

Soumendra N. Bhanja[a], Junye Wang[a,*], Narayan K. Shrestha[a], Xiaokun Zhang[b]

[a] Athabasca River Basin Research Institute (ARBRI), Athabasca University, 1 University Drive, Athabasca, Alberta T9S 3A3, Canada
[b] School of Computing & Information System, Athabasca University, 1 University Drive, Athabasca, Alberta T9S 3A3, Canada

GRAPHICAL ABSTRACT

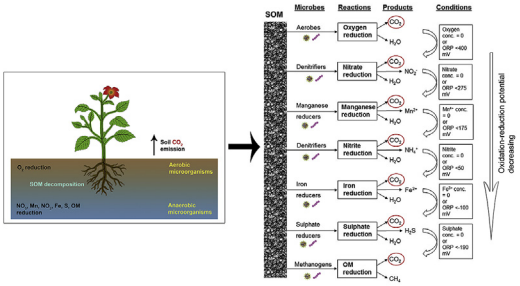

ARTICLE INFO

Keywords:
Carbon
Soil CO_2 emission
Biogeochemical modelling
SWAT-MKT model
Climate change
Watershed model

ABSTRACT

Soil respiration is a crucial source of carbon dioxide (CO_2) in the atmosphere. The underlying processes involved are multifaceted, sequential chemical reactions associated with the conversion of soil organic carbon to CO_2. In this paper, we present a mechanistic, biogeochemical model to simulate soil CO_2 emissions considering the microbial and sequential chemical processes using the well-established hydrological model, Soil and Water Assessment Tool (SWAT) for the first time. The soil CO_2 emissions from multiple sequential soil chemical reactions were compared with the observed data at three sites in Canada. The results show that the modelled CO_2 emission rates are in good agreement with the observed data with performance statistics: PBIAS: 0.13%–23%; NSE: 0.27 to 0.62; RSR: 0.60 to 0.84; R^2: 0.29 to 0.83. This approach could be used in future regional to global-scale models for simulating the soil CO_2 emission and hydrological processes.

1. Introduction

The total carbon storage in soil (2500 Pg up to 1 m depth) is approximately three times higher than atmospheric carbon storage (760 Pg) and more than four times higher than biotic (plants and animals) carbon storage (560 Pg) (Lal, 2008). Therefore, the potential of soil to act as a sink or source of atmospheric greenhouse gases (GHGs) is of great interest (Lal, 2004).

Autotrophic respiration (i.e. tree stem below-ground and root respiration; R_A) and heterotrophic respiration (i.e. soil decomposers; R_H) are the two components of soil respiration (Hanson et al., 2000; Bond-Lamberty et al., 2004; 2018). Soil respiration is one of the major sources of CO_2 in the atmosphere (Ciais et al., 2014), contributing 45–79% of the total ecosystem respiration in forest areas (Brændholt et al., 2018). Soil respiration and the decomposition of soil organic matter (SOM) are not only important processes for the carbon conversion, but also plays a major role in global nutrient dynamics (Manzoni et al., 2008). Therefore, it is necessary to understand the underlying

* Corresponding author.
E-mail address: junyew@athabascau.ca (J. Wang).

https://doi.org/10.1016/j.atmosenv.2019.04.014
Received 27 November 2018; Received in revised form 26 March 2019; Accepted 5 April 2019
Available online 10 April 2019
1352-2310/

processes of soil respiration and the conversion of the soil carbon to CO_2 (Mitchard, 2018). In R_H, soil microorganisms utilize soil organic carbon (SOC) and convert it to CO_2 (Hogberg et al., 2001) and/or methane (CH_4), which poses a potential threat to the global climate (Heimann and Reichstein, 2008). Soil respiration measurements indicate that R_A contributes from 10% to 90% toward the total soil respiration (Hanson et al., 2000; Bond-Lamberty et al., 2018). Contrarily, soil can also act as a terrestrial carbon sink through carbon sequestration (Lal, 2004; Le Quéré et al., 2016). Soil carbon storage is influenced by the availability of nutrients (Wieder et al., 2015). Therefore, an understanding of the dynamics of these soil processes is an important component in predicting the long-term integrity of soil carbon storage and SOM turnover.

A number of attempts have been made over the years to model the soil respiration and/or SOM turnover. However, large discrepancies exist in different earth system models for future soil carbon storage estimation (Todd-Brown et al., 2014). The existing models can be categorized into three types: (1) microbial-ecosystem models (Parnas, 1975; Allison et al., 2010; Wang et al., 2013; Li et al., 2014); (2) coupled reactive transport models (Maggi et al., 2008); and (3) process-based agroecosystem models, such as CENTURY (Parton et al., 1987, 1996), Daycent (Parton, 1996, 1998), DNDC (Li et al., 1992, 2000, 2004), and Roth-C (Jenkinson and Coleman, 2008). A large proportion of these agro-ecosystem models are primarily based on the consideration of the carbon and nitrogen pools, and their turnovers are computed on the basis of their interactions with microbes. However, most of the carbon pool concepts of previous soil CO_2 emission studies do not consider the influence of sequential decomposition of SOM and biogeochemical interactions (Wieder et al., 2013; Le Quéré et al., 2016; Bond-Lamberty et al., 2018). Global carbon emission modelling has been found to improve with the incorporation of the microbial processes (Wieder et al., 2013). Earlier studies have indicated the importance of the sequential redox reactions in soil CO_2 emissions (McBride, 1994; Kirk, 2004; Reddy and DeLaune, 2008). Oxidation reduction potential (ORP, frequently referred to electrochemical potential or redox potential) gradients (positive to negative) can be observed across the depths of submerged soil (Kirk, 2004). The descending ORP gradient can also be formed in soils that are submerged for a longer timescale (Kirk, 2004; Reddy and DeLaune, 2008). The change in ORP patterns govern the availability of electrons in the system (higher electron availability reflects reductive conditions and vice versa) (Stumm and Morgan, 1996; Tan, 2010).

Furthermore, the process-based agroecosystem models are point-based models, leading to difficulties in representing lateral flow modelling. Particularly in watershed modelling, the hydrological processes may be dominant on soil CO_2 emissions. Despite our growing appreciation of the inadequacies of empirically derived C pool concepts for describing soil CO_2 emissions, the most important impediment to improving such empirical models is associated with the complex hierarchy of redox reactions mediated by microbes and their integration with hydrological simulations. Characterization of soil CO_2 emissions has been hampered by the lack of a method for analysis in modelling approaches. As a result, the next generation models of the biogeochemical processes should incorporate “real-world processes” of soil carbon emission (Luo et al., 2016) and include integrated carbon-nutrient dynamics and SOC decomposition (Wieder et al., 2015), and hydrological processes (Shrestha et al., 2018). Therefore, several important issues remain to be addressed in these widely-used process-based agroecosystem models: (1) hierarchical redox reactions, and (2) hydrological processes.

The primary aim of this paper is to develop a detailed mechanistic model for soil respiration processes, and to model the soil sequential chemical reactions and hydrological processes. The watershed-scale model, Soil and Water Assessment Tool (SWAT) has been widely used around the globe for various hydrological and water quality applications (Arnold et al., 1998, 2012; Abbaspour et al., 2015; Meng et al., 2018; Shrestha et al., 2017; Du et al., 2019a, b; Shrestha and Wang, 2018; Shrestha et al., 2018; Wagena et al., 2017). SWAT has the capability of simulating one pool for soil C, N and P, and two separate pools for residue and manure applications (Neitsch et al., 2011). Zhang et al. (2013) have tried to model the soil organic matter dynamics through SWAT in a simplistic, empirical pool-based approach. Previous studies reported soil N_2O modelling through SWAT (Wagena et al., 2017; Yang et al., 2017; Shrestha et al., 2018; Bhanja et al., 2019), however, to our knowledge, no other studies have modelled the soil CO_2 emission using SWAT. Modelling of CO_2 emissions from soils requires to appropriately account for autotrophic respiration and heterotrophic respiration. For the first time, the SWAT model's well defined, process-based hydrology has been used in combination with the newly developed, microbial kinetics and thermodynamics-based MKT model to simulate soil CO_2 emissions. We evaluated the model performance against the comparison with the field-scale data at three Canadian sites.

2. Methodology

2.1. Conceptual model development

Scarcity of oxygen in saturated and semi-saturated soil layers lead to distinct spatio-temporal variability of ORP (McBride, 1994). Various sequential chemical reactions are occurring in this condition mediated by a diverse range of microorganisms such as, aerobes, denitrifiers, manganese reducers, iron reducers, sulfate reducers, and methanogenic bacteria (Patrick and Jugsujinda, 1992; McBride, 1994; Kirk, 2004; Reddy and DeLaune, 2008). These microorganisms follow a thermodynamic sequence of reactions governed by free energy availability; for instance, reactions that are energetically favorable, occurring earlier in this sequence (Bethke et al., 2011). The main controlling factor of geochemical and hydrological cycles is the flow of energy from higher to lower potential (Stumm and Morgan, 1996). The major sequential chemical reactions at the soil-water medium are following (McBride, 1994; Kirk, 2004; Reddy and DeLaune, 2008; Grundl et al., 2011):

$$CH_2O + O_2 \rightleftharpoons CO_2 + H_2O \quad (1)$$

$$CH_2O + 2NO_3^- \rightleftharpoons 2NO_2^- + CO_2 + H_2O \quad (2)$$

$$CH_2O + 2MnO_2 + 4H^+ \rightleftharpoons 2Mn^{2+} + CO_2 + 3H_2O \quad (3)$$

$$3CH_2O + 2NO_2^- + 4H^+ \rightleftharpoons 2NH_4^+ + 3CO_2 + H_2O \quad (4)$$

$$CH_2O + 4Fe(OH)_3 + 8H^+ \rightleftharpoons 4Fe^{2+} + CO_2 + 11H_2O \quad (5)$$

$$2CH_2O + SO_4^{2-} + 2H^+ \rightleftharpoons H_2S + 2CO_2 + 2H_2O \quad (6)$$

$$2CH_2O \rightleftharpoons CH_4 + CO_2 \quad (7)$$

2.2. Framework of the model

The two main components of the model are microbial kinetics and thermodynamics. Availability of a particular chemical species in a system is controlled by ORP condition (Stumm and Morgan, 1996). While, ORP controls the availability of valence state of an ion, reaction catalysis is controlled by the microbial kinetics. Microorganisms are the driving factors for SOM decomposition and the associated processes at a particular ORP state (Equations (1)–(7)). The conceptual SOM decomposition steps are shown in Fig. 1. It is important to note that the incorporation of MKT model into the SWAT framework enabling the modelling of spatio-temporal water transport components using the corresponding submodules of SWAT.

2.3. Processes involving microbial kinetics

The dual Michaelis-Menten kinetics have been used to decipher the microbial kinetics (van Bodegom and Scholten, 2001; Davidson et al., 2012; Jin and Kirk, 2016; Bhanja et al., 2019). The reaction rate (R in

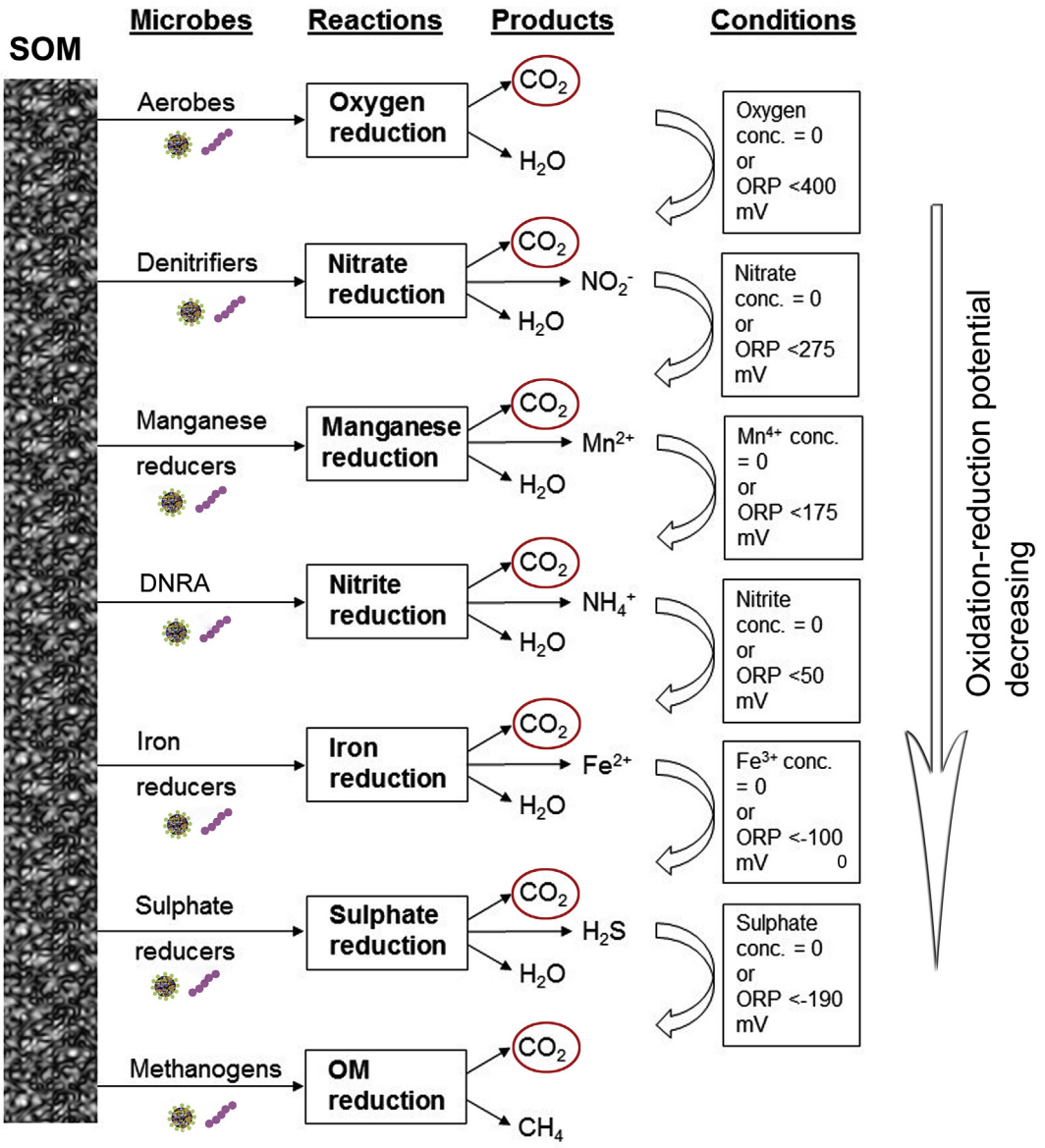

Fig. 1. The MKT model processes. Soil CO_2 emissions from different sequential reactions are shown with red circle. DNRA: Dissimilatory Nitrate Reduction to Ammonium. (For interpretation of the references to colour in this figure legend, the reader is referred to the Web version of this article.)

molal/day) can be expressed as:

$$R = Q_{max}.\ B.\ \frac{[ED]}{K_D + [ED]}.\ \frac{[EA]}{K_A + [EA]} \tag{8}$$

Where, Q_{max} is the specific microbial activity of biomass per day (mol/mol/day); B the microbial biomass (mol/l); $[ED]$ the concentration of the electron donor species (molal); $[EA]$ is the concentration of the electron acceptor (molal); and K_D and K_A are the half saturation constants for the organic matter and the electron acceptors, respectively (mol/l). Electron acceptor (EA) and electron donor substrates are the substrates used in Michaelis-Menten kinetics. Due to its chemical nature, SOM has been considered as an electron donor (Lovley and Philips, 1986; Lovley, 1987, 2008; Postma and Jakobsen, 1996). The other species' in Equations (1)–(6) are acting as an electron acceptor to complete a redox couple in a reaction sequence (Half- and complete cell reactions are shown in Table 1). $[ED]$ is replaced as $[OM]$ to represent the SOM molal concentration. We have rearranged equation (8) to obtain the $[EA]$ concentration:

$$[EA] = \frac{K_A.\ R.\ (K_D + [OM])}{V_{max}.\ [OM] + R.\ (K_D + [OM])} \tag{9}$$

Where, $V_{max} = Q_{max}\ .\ B$ (van Bodegom and Scholten, 2001).

2.4. Processes governed by thermodynamics

A redox reaction can be written in the following form:

$$xA + yD \rightleftharpoons pA^{-} + qD^{+} \tag{10}$$

Where, A and A^- are the electron acceptor species and its reduced form, respectively. D and D^+ are the elector donor species and its oxidized form, respectively. x, y, p and q, are the stoichiometric coefficients of reactants and products, respectively.

The dynamic oxidation-reduction potential in the medium, has been estimated following the Nernst's equation (Stumm and Morgan, 1996).

$$E = E^0 + \frac{R.\ T}{n.\ F} \ln \frac{1}{Q} \tag{11}$$

Where, E is the oxidation-reduction potential (mV); E^0 is the

Table 1
Half cell reactions, complete cell reactions, standard ORP (mV) at pH = 7 and 25 °C (following Bratsch, 1989; Stumm and Morgan, 1996; Reddy and DeLaune, 2008) and the number of electrons transferred.

Reactions	E^0 mV	E^0 total mV	Electrons transferred
$O_2\,(g) + 4H^+(aq) + 4e^- \rightleftharpoons 2H_2O(l)$	810		4
$CH_2O(aq) + H_2O\,(l) \rightleftharpoons CO_2(g) + 4H^+(aq) + 4e^-$	-(-180)		
$CH_2O(aq) + O_2(g) \rightleftharpoons CO_2(g) + H_2O(l)$		990	
$2NO_3^-(aq) + 4H^+(aq) + 4e^- \rightleftharpoons 2NO_2^-(aq) + 2H_2O(l)$	410		4
$CH_2O(aq) + H_2O(l) \rightleftharpoons CO_2(g) + 4H^+(aq) + 4e^-$	-(-180)		
$CH_2O(aq) + 2NO_3^-(aq) \rightleftharpoons 2NO_2^-(aq) + CO_2(g) + H_2O(l)$		590	
$2MnO_2(aq) + 8H^+(aq) + 4e^- \rightleftharpoons 2Mn^{2+}(aq) + 4H_2O(l)$	870		4
$CH_2O(aq) + H_2O(l) \rightleftharpoons CO_2(g) + 4H^+(aq) + 4e^-$	-(-180)		
$CH_2O(aq) + 2MnO_2(aq) + 4H^+(aq) \rightleftharpoons 2Mn^{2+}(aq) + CO_2(g) + 3H_2O(l)$		1050	
$2NO_2^-(aq) + 16H^+(aq) + 12e^- \rightleftharpoons 2NH_4^+(aq) + 4H_2O(l)$	470		12
$3CH_2O(aq) + 3H_2O(l) \rightleftharpoons 3CO_2(g) + 12H^+(aq) + 12e^-$	-(-180)		
$3CH_2O(aq) + 2NO_2^-(aq) + 4H^+(aq) \rightleftharpoons 2NH_4^+(aq) + 3CO_2(g) + H_2O(l)$		650	
$4Fe(OH)_3\,(aq) + 12H^+(aq) + 4e^- \rightleftharpoons 4Fe^{2+}(aq) + 12H_2O(l)$	380		4
$CH_2O(aq) + H_2O(l) \rightleftharpoons CO_2(g) + 4H^+(aq) + 4e^-$	-(-180)		
$CH_2O(aq) + 4Fe(OH)_3(aq) + 8H^+(aq) \rightleftharpoons 4Fe^{2+}(aq) + CO_2(g) + 11H_2O(l)$		560	
$SO_4^{2-} + 10H^+(aq) + 8e^- \rightleftharpoons H_2S + 4H_2O(l)$	-80		8
$2CH_2O(aq) + 2H_2O(l) \rightleftharpoons 2CO_2(g) + 8H^+ + 8e^-$	-(-180)		
$2CH_2O(aq) + SO_4^{2-}(aq) + 2H^+(aq) \rightleftharpoons H_2S(g) + 2CO_2(g) + 2H_2O(l)$		100	
$CO_2(g) + 8H^+(aq) + 8e^- \rightleftharpoons CH_4(g) + 2H_2O(l)$	-250		8
$2CH_2O(aq) + 2H_2O(l) \rightleftharpoons 2CO_2(g) + 8H^+(aq) + 8e^-$	-(-180)		
$2CH_2O(aq) \rightleftharpoons CH_4(g) + CO_2(g)$		-70	

standard electrode potential (mV); *R:* the universal gas constant ($J.mol^{-1}.K^{-1}$); *T*: absolute temperature (kelvin); *n*: the number of electrons transferred (mol); *F:* the Faraday's constant (Coulomb); and *Q:* the reaction quotient.

At 25 °C, Equation (11) simplifies to:

$$E = E^0 + \frac{59.3}{n}\log\frac{1}{Q} \tag{12}$$

In Equation (11), *Q* for Equation (10) can be expressed as:

$$Q = \frac{[A^-]^p.\,[D^+]^q}{[A]^x.\,[D]^y} \times \frac{\gamma_{A^-}^{p}.\,\gamma_{D^+}^{q}}{\gamma_A^x.\,\gamma_D^y} \tag{13}$$

Where, '[ ]' represents the species' concentration (molal) and 'γ' represents the activity coefficients (molal). More details on the reaction quotient can be obtained from Stumm and Morgan (1996). Reaction specific reaction quotient values are provided in Table S1.

E^0 values at pH 7 and 25 °C are compiled from Bratsch (1989), Stumm and Morgan (1996), Reddy and DeLaune (2008). For some of the reaction sequences, the E^0 values is given for other pH values instead of 7. We estimated the E^0 for pH 7 following (Gliński and Stepniewski, 1985; Pidello, 2003; Quin et al., 2015):

$$E^0_{pH=7} = E^0 - \frac{R.\,T}{F} \times ln10\ \times (7 - pH) \tag{14}$$

At 25 °C, Equation (14) simplifies:

$$E^0_{pH=7} = E^0 - 59.3 \times (7 - pH) \tag{15}$$

2.5. Modelling the redox disequilibrium

The reaction follow thermodynamic laws, i.e. the Nernst equation in redox equilibrium (Stumm and Morgan, 1996). One of the drawbacks of the equilibrium model - it occasionally reveals the chemical states in natural system (Bethke, 2007). Equations (11) and (12) are based on redox equilibrium, however, the natural systems are not always follow the redox equilibrium (Stumm and Morgan, 1996; Bethke, 2007). Microorganisms take advantage of the redox disequilibrium conditions for their respiration and are catalyzing the electron transfers (Bethke, 2007). Microbial energy uptake has to be considered in the model processes to accurately conserve the energy (Jin and Bethke, 2005; Jin and Kirk, 2016). The change in Gibb's free energy for a microbial process (ΔG_m) has been estimated following (Jin and Bethke, 2005; Jin and Kirk, 2016):

$$\delta G_m = m_p.\,\delta G_p \tag{16}$$

Where, m_p is the microbial ATP yield (mol); ΔG_p: the phosphorylation energy (= 45–48 kJ/mol). For aerobic processes (Equation (1)), the phosphorylation energy has been considered as 48 kJ/mol, else it is considered as 45 kJ/mol (Jin and Bethke, 2005; Jin and Kirk, 2016). m_p values are dependent on the nature of the reaction and are obtained from Jin and Bethke (2005), Jin and Kirk (2016). The oxidation-reduction potential change due to microbial activity (E_m) becomes:

$$E_m = \frac{\delta G_m}{n\ .\ F} \tag{17}$$

Finally, the net oxidation-reduction potential (E') is estimated on a daily basis following the equation:

$$E' = E - E_m \tag{18}$$

2.6. Influence of temperature on the reaction rates

The SOM decomposition process is very sensitive to temperature fluctuations (Davidson and Janssens, 2006). A temperature (Q_{10}) coefficient has been used to represent the temperature sensitivity. Q_{10} is estimated as the increase of reaction rate for a 10 °C rise in temperature (Davidson and Janssens, 2006). Experiments report Q_{10} values of a magnitude 2 to 3 at soil temperature near room temperature (Van't Hoff and Lehfeldt, 1899). The reaction-specific Q_{10} values are obtained from literature (Table 2). New reaction rates (R') are computed following:

$$R' = R.\,Q_{10}^{\frac{SoilT-30}{10}} \tag{19}$$

Where, SoilT represents soil temperature (°C).

2.7. The Soil and Water Assessment Tool (SWAT)

The Soil and Water Assessment Tool (SWAT) (Arnold et al., 1998) model has been used to simulate daily-scale soil water-filled pore

Table 2
Parameters used for simulating reaction-specific microbial kinetics. Units used for *Rate* and $Rate_{max}$: molal/day; K_m and K_D: molal, respectively.

Reactions	Parameters	Values	Calibrated value	References
Oxygen reduction	*Rate*	1.00×10^{-3} to 24.00×10^{-3}	1.00×10^{-3}	Noll et al. (2005); Davidson et al. (2012)
	$Rate_{max}$	1.04×10^{-2}	1.04×10^{-2}	Van Bodegam and Scholten (2001)
	K_m	0.121	0.121	Davidson et al. (2012)
	K_D	4.00×10^{-4}	4.00×10^{-4}	Davidson et al. (2012)
	Q_{10}	2.9	2.9	Davidson et al. (2012)
Nitrate reduction	*Rate*	5.00×10^{-5} to 9.30×10^{-3}	1.00×10^{-4}	Goreau et al. (1980); Dangelo and Reddy (1999)
	$Rate_{max}$	1.04×10^{-2}	1.04×10^{-2}	Van Bodegam and Scholten (2001)
	K_m	4.20×10^{-4}	4.20×10^{-4}	Bradley et al. (1998)
	K_D	9.00×10^{-5}	9.00×10^{-5}	Van Bodegam and Scholten (2001)
	Q_{10}	2.0	2.0	Hartwig et al. (2002)
Manganese reduction	*Rate*	1.00×10^{-5}	1.00×10^{-5}	Goreau et al. (1980)
	$Rate_{max}$	1.10×10^{-4} to 1.04×10^{-2}	1.10×10^{-4}	Peters and Conrad (1996); Van Bodegam and Scholten (2001)
	K_m	4.20×10^{-4}	4.20×10^{-4}	Bradley et al. (1998)
	K_D	9.00×10^{-5}	9.00×10^{-5}	Van Bodegam and Scholten (2001)
	Q_{10}	2.0	2.0	Hartwig et al. (2002)
Nitrite reduction	*Rate*	1.00×10^{-4}	1.00×10^{-4}	Goreau et al. (1980)
	$Rate_{max}$	1.04×10^{-2}	1.04×10^{-2}	Van Bodegam and Scholten (2001)
	K_m	1.26×10^{-6}	1.26×10^{-6}	Bradley et al. (1998)
	K_D	9.00×10^{-5}	9.00×10^{-5}	Van Bodegam and Scholten (2001)
	Q_{10}	2.0	2.0	Hartwig et al. (2002)
Iron reduction	*Rate*	2.00×10^{-3} to 3.00×10^{-2}	2.00×10^{-3}	Ginn et al. (2017)
	$Rate_{max}$	9.40×10^{-4} to 4.33×10^{-2}	4.33×10^{-2}	Peters and Conrad (1996); Van Bodegam and Scholten (2001); Ginn et al. (2017)
	K_m	6.50×10^{-6}	6.50×10^{-6}	Jin and Kirk (2016)
	K_D	1.20×10^{-5}	1.20×10^{-5}	Jin and Kirk (2016)
	Q_{10}	2.4	2.4	Van Bodegam and Stams (1999)
Sulphate reduction	*Rate*	1.00×10^{-5} to 1.11×10^{-2}	1.00×10^{-5}	Dangelo and Reddy (1999); Pallud and van Cappellen (2006)
	$Rate_{max}$	8.90×10^{-5} to 6.92×10^{-4}	8.90×10^{-5}	Peters and Conrad (1996); Van Bodegam and Scholten (2001); Pallud and van Cappellen (2006)
	K_m	1.00×10^{-4} to 6.80×10^{-5}	6.80×10^{-5}	Pallud and van Cappellen (2006); Jin et al. (2013)
	K_D	7.90×10^{-4}	7.90×10^{-4}	Van Bodegam and Scholten (2001)
	Q_{10}	1.6	1.6	Van Bodegam and Stams (1999)
Organic matter reduction	*Rate*	1.00×10^{-6}	1.00×10^{-6}	Goreau et al. (1980)
	$Rate_{max}$	2.00×10^{-4} to 5.10×10^{-4}	2.00×10^{-4}	Peters and Conrad (1996); Van Bodegam and Scholten (2001)
	K_m	6.80×10^{-5}	6.80×10^{-5}	Jin et al. (2013)
	K_D	5.00×10^{-6}	5.00×10^{-6}	Van Bodegam and Scholten (2001)
	Q_{10}	4.6	4.6	Van Bodegam and Stams (1999)

fraction (WFPF) and soil temperature. Details of SWAT's hydrology processes can be found in Arnold et al. (1998) and Neitsch et al. (2011). There are two major approaches for SWAT model setup: build the model and perform calibration and validation for the entire study region; and utilize the location-specific information in a pre-existing model for calibration and validation purpose (Srinivasan et al., 2010; Zhang et al., 2013; Shrestha et al., 2017; Shrestha et al., 2018; Shrestha and Wang, 2018). The second approach may provide a comparatively lesser model performance but deliver a more objective assessment (Zhang et al., 2013). The second approach is more effective for a lesser number of site-scale measurements availability. The sites used for calibration/validation represent a very small fraction of the total terrestrial area (Zhang et al., 2013). We used a SWAT model set up by Shrestha et al. (2017) for the Athabasca River Basin (ARB) in Alberta, Canada and used site-specific soil information, meteorological information such as precipitation, air temperature, soil physical properties, and soil nutrient concentrations etc. at three sites in similar cold climate regions from Amadi et al. (2016) (refer section 2.8 for details).

2.8. Field-scale CO_2 emission data

As CO_2 measurements are unavailable inside the ARB, three sites were selected for calibration and validation from Amadi et al. (2016) in Saskatchewan, Canada (Fig. S1). The three sites, namely, Outlook and Saskatoon are located in prairie ecozone and Prince Albert is located in boreal plain ecozone. Dark brown to black Chernozem soils are indigenous to the region. The region is subjected to a semi-arid temperate climate with annual precipitation varying from 181 to 466 mm/yr. The rectangular gas chambers were installed at a depth of 5 cm to collect the gas samples for a total of 30 min time. The vegetation within the chambers was removed before sampling. Gas sampling has been done in 10 min interval within the 30 min. In order to get the day-scale estimate, regression analysis has been performed based on the available data. Four gas chambers were placed at each site at a distance of 20 m. The CO_2 emission data from three shelterbelt sites were available in 2013 and 2014. Soil moisture and soil temperature observations were carried out at the field using a digital soil moisture meter and a digital thermometer, respectively. These measurements were done at a depth of 10 cm. This gas sampling process has been carried out twice a week between spring thaw until freezing of soil. Detailed descriptions can be found in Amadi et al. (2016).

2.9. Soil respiration computation through SWAT-MKT model

MKT model is written in FORTRAN language and integrated with the SWAT framework (along with other SWAT subroutines) for a coupled simulation of soil CO_2 emission. Like all other major SWAT subroutines, it is operating at daily scale with a possibility to sub-daily simulations in future. MKT requirements of meteorological parameters such as, soil temperature and soil moisture are used directly from the SWAT simulation. Regional-scale simulation capabilities of SWAT is also a positive aspect of SWAT-MKT model.

R_H and R_A are the two major components of the soil respiration. R_H is simulated here based on the sequential chemical reactions occurring at the soil-water medium. Soil CO_2 emission is simulated in different soil layers. The first soil layer (10 mm) is considered as aerobic only. Daily-scale soil CO_2 emission is estimated as the bi-product of the chemical reactions (Equations (1)–(7); Fig. 1). Field-scale measurement data of R_A is not available at the study region. Hanson et al. (2000) reported that a fraction of 10–90% of total soil respiration can be

attributed to R_A. Li et al. (1994) indicated that R_A is a combination of three processes: (1) root growth, (2) root maintenance, and (3) ion uptake and transport. Root growth is a variable of plant growth model in SWAT and is updated daily to represent the root biomass growth. However, the other two processes are difficult to simulate through SWAT at present. To compare the model simulated data with field-scale data (soil CO_2 emission), R_A data are obtained from Hanson et al. (2000) and Bond-Lamberty et al. (2004, 2018) and used after tuning.

Unit conversion for soil respiration from molality/day to kg/ha/day is done following the equation:

$$x = x.\ BD.\ z.\ M.\ \ WFPF.\ por \tag{20}$$

Where, *BD*: soil bulk density (g/cm^3); *z*: soil layer thickness (cm); M: molecular weight of CO_2 (44 g/mol); *WFPF*: water-filler pore fraction (fraction); *por*: soil porosity fraction (fraction).

2.10. Statistical considerations

The following statistical approaches have been used for comparison between observed and simulated WFPF, soil temperature and CO_2 emissions. Percent bias (PBIAS), Nash-Sutcliffe efficiency (NSE), and root mean square error (RMSE) to standard deviation ratio (RSR), are used as the major statistical indexes for the model performance (Moriasi et al., 2007). PBIAS indicate the average deviation of the model simulated output from the observed values (Gupta et al., 1999). The ratio of residual variance and data variance is represented by NSE (Nash and Sutcliffe, 1970).

$$\text{PBIAS} = \frac{\sum_{i=1}^{n}(x_i - y_i) \times 100}{\sum_{i=1}^{n} x_i} \tag{21}$$

$$\text{NSE} = 1 - \left[\frac{\sum_{i=1}^{n}(x_i - y_i)^2}{\sum_{i=1}^{n}(x_i - \bar{x})^2}\right] \tag{22}$$

$$RSR = \frac{\sqrt{\sum_{i=1}^{n}(x_i - y_i)^2}}{\sqrt{\sum_{i=1}^{n}(x_i - \bar{x})^2}} \tag{23}$$

Where, x_i represents the observed values; y_i represents the simulated values; i (= 1, 2, 3, …, n) indicate the number of data points; $\bar{x}$ and $\bar{y}$ represent mean values. The Pearson's correlation coefficient (R), RMSE and the mean absolute error (MAE) have been estimated to show the departure of model estimates from the observed values (Helsel and Hirsch, 1992; Moriasi et al., 2007).

$$\text{Pearson's correlation (R)} = \frac{\sum_{i=1}^{n}(x_i - \bar{x})(y_i - \bar{y})}{\sqrt{\sum_{i=1}^{n}(x_i - \bar{x})^2}\sqrt{\sum_{i=1}^{n}(y_i - \bar{y})^2}} \tag{24}$$

$$\text{RMSE} = \sqrt{\sum_{i=1}^{n}\frac{(x_i - y_i)^2}{n}} \tag{25}$$

$$\text{MAE} = \frac{\sum_{i=1}^{n}|x_i - y_i|}{n} \tag{26}$$

Outliers present in the observed data are investigated through Tukey's fence approach (Tukey, 1977). Lower bound and upper bound in the data are represented as:

$$\text{Lower bound} = Q_1 - (Q_3 - Q_1) \times 1.5 \tag{27}$$

$$\text{Upper bound} = Q_3 + (Q_3 - Q_1) \times 1.5 \tag{28}$$

Where, Q_3 and Q_1 are the 3rd and the 1st quartile in the data distribution, respectively. The values located beyond the lower or upper bound are characterized as outliers.

2.11. Sensitivity and calibration analyses

One factor at a time (OFAT) approach has been followed to perform sensitivity analysis (Hamby, 1994). A sensitivity index has been computed to indicate the parameters that are mostly controlling the magnitude of the outputs (Table S3). Sensitivity index (SI) has been estimated following Hamby (1994):

$$SI = \frac{val_{high} - val_{low}}{val_{high}} \tag{29}$$

Where, the lowest to highest output values are represented as val_{low} and val_{high}, respectively.

Parameters that were calibrated for WFPF and soil temperature simulations are shown in Table S3. Parameters that were calibrated for soil CO_2 emission simulation are shown in Table 2. Based on the data availability, daily field-scale observations in 2013 are used for calibration at the three Canadian sites, Outlook, Saskatoon and Prince Albert.

2.12. Assumptions of the soil CO_2 emission modelling through MKT application

It is difficult to estimate the uncertainty associated with any of the parameters used for the modelling (Table 2). Whenever the values of some of the parameters are not available in previous literature, we used the values for the nearest available reaction(s). To model the complex chemical processes we use the assumptions of one-step reactions to preserve computational efficiency (McBride, 1994; Reddy and DeLaune, 2008). Thus, the sequential reactions are modelled to be undergone successively once at a time in the initial version of the model. In real field processes, microbial and chemical reactions depend on availability and kinetics of the reactants. This might introduce uncertainty because soil microbial heterogeneity cannot be resolved in field scale at present. Chemical mass balance are computed by converting the species concentration to molality. SOM is composed of several elements with complex chemical structure. One mole of SOM has been converted to 1 mol of CH_2O that can act as electron donor in the reactions. A molecular weight of 23300 g/mol for SOM has been used here following Louie et al. (2013). This means approximately 30 g of active CH_2O can come to solution from 23300 g of SOM. The assumption is in line with the observations of Magill and Aber (2000), which reports 0.2–6 mg of DOC-C can be originated per g of initial litter mass. In the initial version of the model, atmospheric diffusion is not considered. The soil temperature and WFPF values are obtained from SWAT simulation and used directly in the MKT model simulation. Hydrologic fluxes are not influencing the reactants and products. Initial concentrations of different chemical species used are provided in Table S4. We used the dissolved initial concentration of 1.0×10^{-9} molal for H_2S and CH_4. Users can use their own reaction specific, experimental values in the model. The MKT model simulation can be improved further in future by calculating the dissolved gases after incorporating Raoult's law, Fugacity and Henry's law (Stumm and Morgan, 1996; Mackay, 2001; Sander, 2015).

3. Results and discussions

3.1. Water filled pore fraction and soil temperature simulation

As the WFPF and soil moisture data are simulated using the SWAT model, we show the calibration and validation for these two parameters. Overall, the simulated WFPF has well represent the wetting of soil after precipitation event or during the snowmelt event in April–May (Fig. 2). The simulated WFPF show “good” to “very good” model evaluation statistics (PBIAS, NSE, RSR, R^2, RMSE and MAE) during the calibration period in all of the studied locations (Fig. 2). Simulated

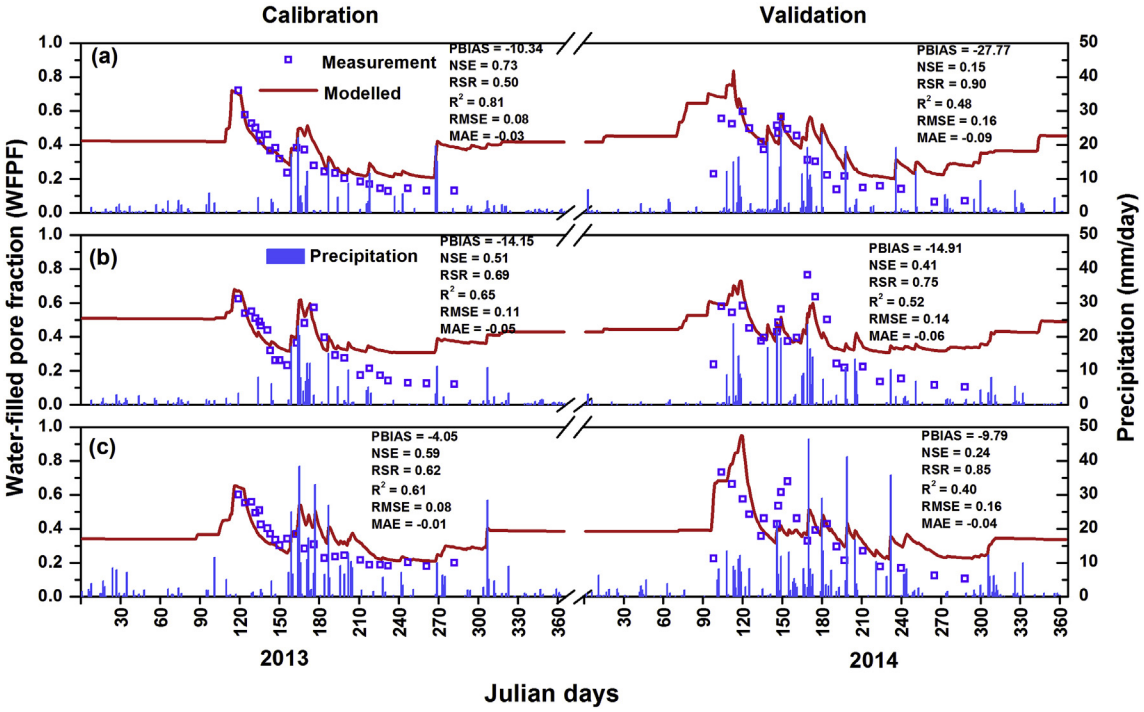

Fig. 2. In situ measured and modelled daily water-filled pore fraction (WFPF) at (a) Outlook, (b) Saskatoon and (c) Prince Albert. Precipitation data are shown in column.

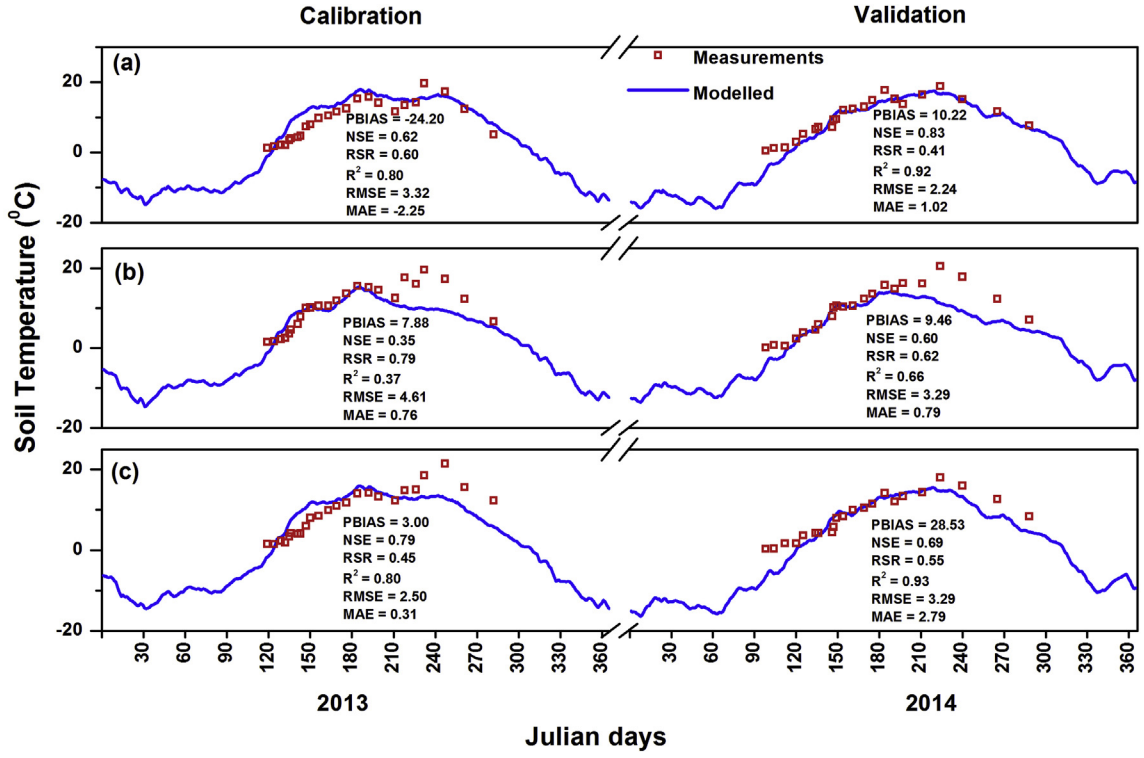

Fig. 3. Daily-scale, in situ measured and modelled soil temperature at (a) Outlook, (b) Saskatoon and (c) Prince Albert.

WFPF also indicate "satisfactory" to "very good" match in terms of model evaluation statistics during the validation period (Fig. 2). Model estimated WFPF sometime overestimated the observed value at the Saskatoon site, particularly during dry periods (Fig. 2). Presence of higher clay fraction (~47%; Amadi et al., 2016) in soil at Saskatoon location might be a major reason for the overestimation. Water holding capacity increases with higher clay fraction and it is also represented in the model simulation. Simulated daily soil temperature data show "satisfactory" to "very good" model evaluation statistics during both the calibration and validation period (Fig. 3). Model output show some underestimations on comparing with the observed estimates at Saskatoon and Prince Albert sites (Fig. 3).

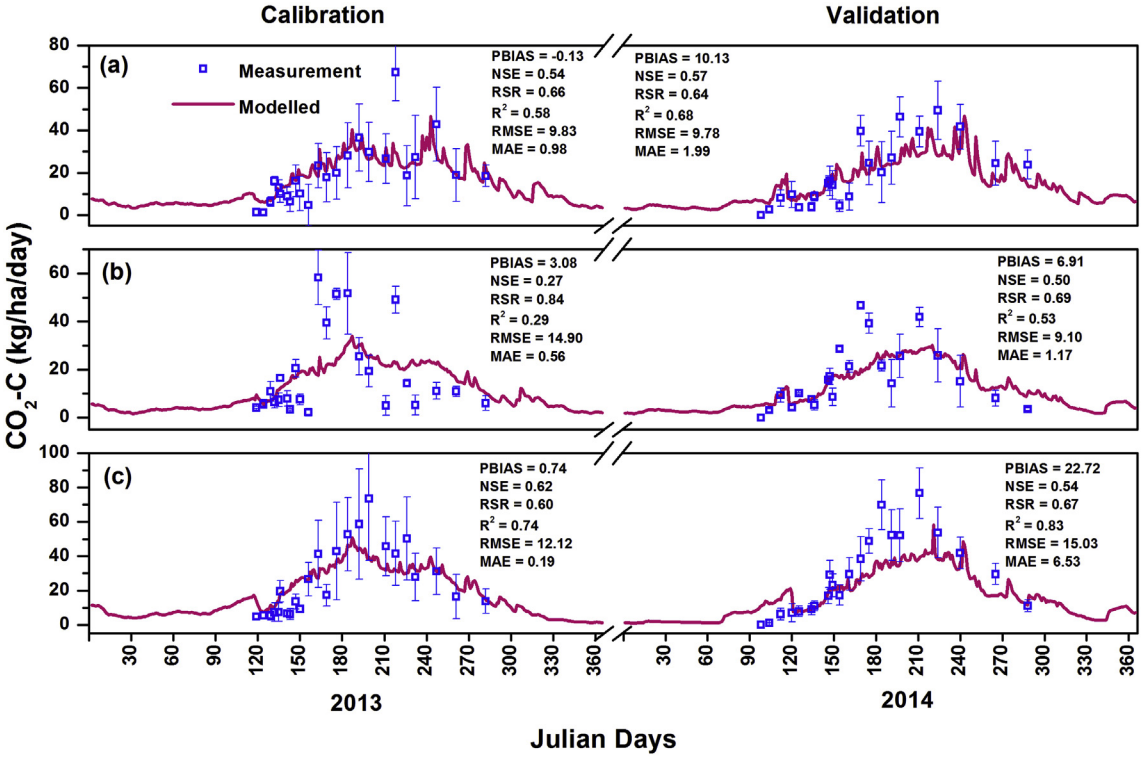

Fig. 4. Daily-scale, in situ measured and modelled soil CO_2 emission at (a) Outlook, (b) Saskatoon and (c) Prince Albert.

3.2. Soil CO_2 emission modelling

Oxygen reduction rate and maximum rate for organic matter reduction are found to be the two most sensitive parameters for controlling the CO_2 emission from soil (Table S2). Although CO_2 is a by-product of all of equations (1)–(7) mentioned above, favorable reaction *rate* in combination with the $rate_{max}$, K_m, K_D and Q_{10} values are influencing factors for observation of high sensitivity of soil CO_2 emission to oxygen reduction processes. Secondly, stoichiometric coefficients also play crucial role in the sensitivity analysis. For example, 1 mol of $Fe(OH)_3$ can only produce 0.25 mol of CO_2 following Equation (5). Thirdly, soil CO_2 emission includes emissions from all of the soil layers, within which, the aerobic, first soil layer contributes significantly to total CO_2 emission.

Observed soil CO_2 emission shows higher values during summertime (Fig. 4). Simulated soil CO_2 emission reflects the similar trend as of the observed one (Fig. 4). In general, the magnitude and patterns of the simulated values match well with the observed values during calibration and validation period in all of the three sites studied (Fig. 4). The daily-scale, simulated values show "very good" model performance statistics in Outlook and Prince Albert sites during calibration period (Fig. 4). Model simulated daily-scale, CO_2 emission indicate "good" to "very good" performance statistics (PBIAS ranged within 23; NSE varies from 0.5 to 0.57; RSR varies from 0.64 to 0.69) during validation period at all of the three sites studied (Fig. 4). The model results underestimated the observed values during spring time for some of the measurement days, it is interesting to note that the model outputs are within the uncertainty band of the observed estimates in most of the days (Fig. 4). The outliers in observed data influence the evaluation statistics, particularly at the Outlook and the Prince Albert sites (Fig. 4). Removal of these outliers might improve the statistics, but we keep those for consistency. The observation was based on the gas sampling once a day for 30 min. Then it was converted to daily-scale emission estimates by fitting linear or exponential regression equations to the concentration vs. time data. Thus, gas sampling for 30 min and its conversion to daily-scale estimates might be a reason for the mismatch. Furthermore, R_A is a crucial component on comparing with the field-scale estimates. However, due to the unavailability of direct field-scale measurements of R_A, we calculate R_A using indirect data of the ratio between heterotrophic respiration to the soil respiration from Hanson et al. (2000) and Bond-Lamberty et al. (2004, 2018). R_A accounts for 10%–90% of the total soil respiration (Hanson et al., 2000; Bond-Lamberty et al., 2018). After comparing with field-scale soil CO_2 emission data of 2013, we used a value of 76% contribution of R_A for estimating total soil respiration. R_A data could lead to uncertain total soil CO_2 emission estimates and hence, it might be a reason for the mismatch.

We investigate the model performance further following the scatter analyses of the modelled and observed estimates (Fig. 5). In general, the scatters are found closer to the 1:1 line during the entire study period at the three locations. The outliers are indicated through Tukey's fence approach (Tukey, 1977). Outliers are observed during calibration period at the Outlook and Saskatoon sites. This is the reason for obtaining comparatively better match during validation period at Outlook and Saskatoon (Fig. 4). Model statistics show better match of soil CO_2 emission than the earlier study in the same region (Yadav and Wang, 2017). They used DNDC model to simulate soil CO_2 emission in agricultural region of the same three sites and observed the following model statistics: R^2: 0.09 to 0.55 and RMSE: 4.3 to 19.1. Although soil CO_2 emissions were simulated using microbial kinetics and thermodynamics within the DNDC model (Li et al., 2004, 2005), their redox calculations are considered only for the ORP simulation instead of chemical mass balance and kinetics approach due to simplified hydrological processes of the DNDC. Because of the improved hydrological parameterization in the SWAT, the present results are better than the DNDC. Particularly, soil CO_2 emission can be simulated at a regional-scale straightforward with the coupling within the SWAT framework**.** Regional-scale simulation of soil CO_2 emission shows spatio-temporal variations across the sub-basins in the Athabasca river basin (Fig. 6). Higher CO_2—C emission values are observed during summer months, on the other hand, lowest values (< 50 kg/ha/month) are observed in most of the sub-basins during winter months, December to April (Fig. 6).

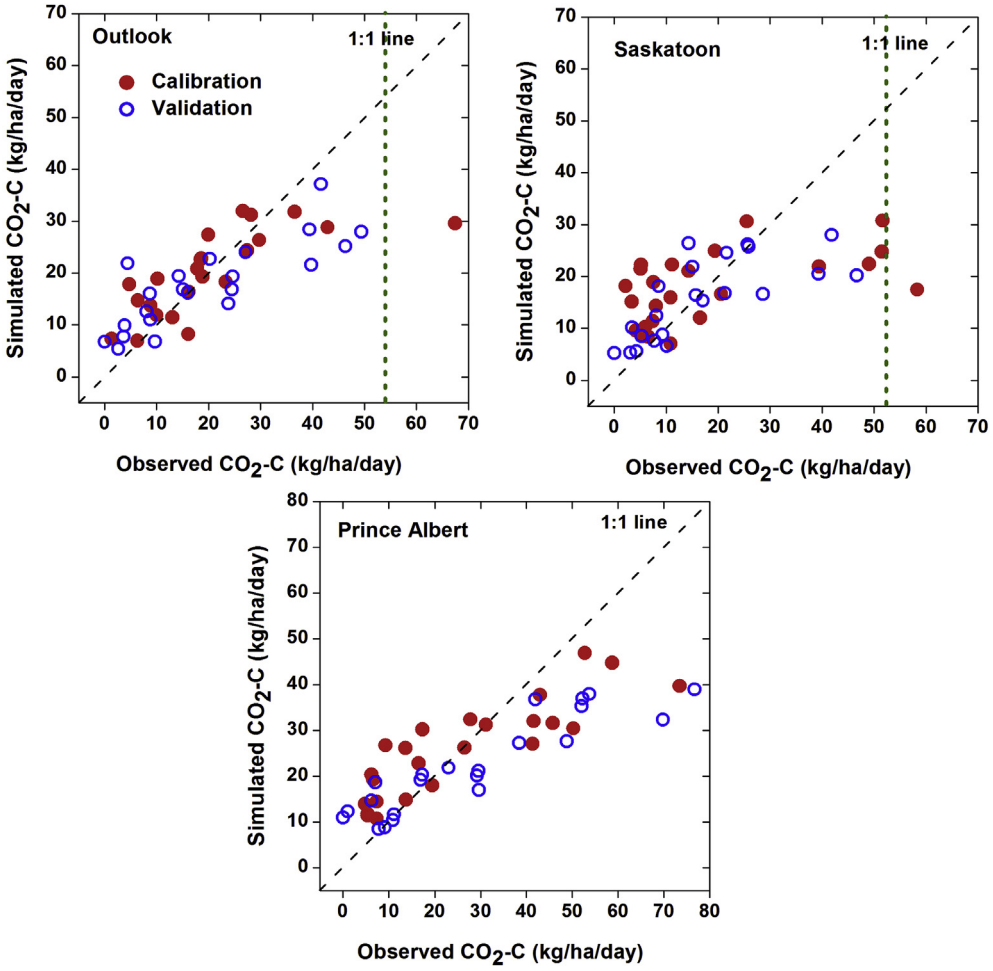

Fig. 5. Scatter analyses for simulated and observed soil CO_2 emission during calibration (red filled circles) and the validation period (blue open circles). Dotted line indicate the upper bounds (if located within the axis limit) of Tukey's fence (Tukey, 1977). (For interpretation of the references to colour in this figure legend, the reader is referred to the Web version of this article.)

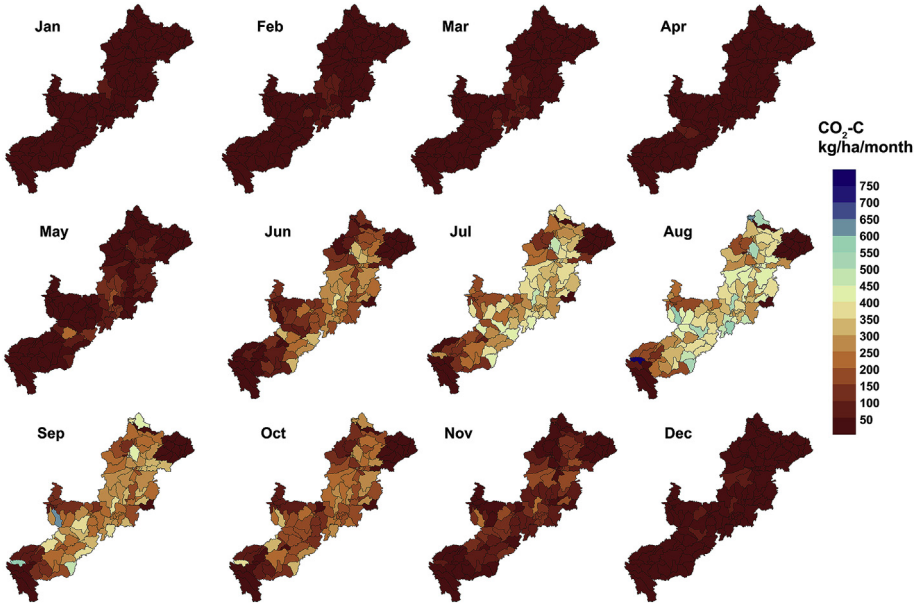

Fig. 6. Seasonal soil CO_2 emissions in Athabasca river basin in 2013.

3.3. Advantages of the SWAT-MKT model

MKT model has numerous advantages for simulating soil CO_2 emission comparing the traditional pool-based models (e.g. carbon pool, nitrogen pool etc.). The consideration of sequential chemical reactions has been enabling the exact representation of chemical environment at the soil water zone. The model can be used to simulate the spatio-temporal variations in soil ORP values. Li et al. (2004) attempted to model site-scale, soil GHG emissions using microbial kinetics and thermodynamics through DNDC model. However, they have considered only empirical equations for the ORP simulation instead of chemical mass balance and kinetics approach. Yan et al. (2018) has studied the influence of soil moisture for soil CO_2 emission modelling as a proxy of anaerobic environment. They used soil moisture as a representative of anaerobic nature of the medium. On the contrary, MKT model simulation enable users to model ORP dynamics in the soil-water medium and soil CO_2 emission simultaneously. The use of regional-scale hydrology through SWAT and incorporating the detailed redox-based chemical processes are the major advantages of the proposed SWAT-based MKT model. The integrated model simulation enable users to perform multiple, watershed-scale hydrological and biogeochemical operations at one run.

4. Conclusions

Regional-scale soil CO_2 emission modelling has been performed through a newly developed MKT model. The biogeochemical transformation of soil organic matter and other chemical compounds in the model is based on microbial kinetics and thermodynamics. The undergoing soil chemical reactions are modelled for the first time through SWAT tool and CO_2 production from each of these reactions are considered. SWAT-based MKT model accounts appropriately for autotrophic respiration and heterotrophic respiration for modelling of CO_2 emissions from soils. The coupled model's performance has been evaluated in terms of soil CO_2 emission simulation in 2013–2014 against field-scale data from three Canadian sites, Outlook, Saskatoon and Prince Albert. The results show that the simulated CO_2 fluxes were in good agreement with the observed data in terms of statistical performances (PBIAS: 0.13 to 23; NSE: 0.27 to 0.62; RSR: 0.60 to 0.84; R^2: 0.29 to 0.83) in all of the three studied sites. Due to its capability for simulating multiple applications of integrated biogeochemical and hydrological processes at one run, we believe, the MKT model can be widely used in regional to global scale models for air-soil-water quality applications in future.

Acknowledgement

The authors would like to thank the Alberta Economic Development and Trade for the Campus Alberta Innovates Program Research Chair (No. RCP-12-001-BCAIP). Soil CO_2 data from the three sites are taken from Amadi et al. (2016), we acknowledge their effort for making the data available to use. We acknowledge RAMP for providing the water quality data.

Appendix A. Supplementary data

Supplementary data to this article can be found online at https://doi.org/10.1016/j.atmosenv.2019.04.014.

References

Abbaspour, K.C., Rouholahnejad, E., Vaghefi, S., Srinivasan, R., Yang, H., Klove, B., 2015. A continental-scale hydrology and water quality model for Europe: calibration and uncertainty of a high-resolution large-scale SWAT model. J. Hydrol. 524, 733–752.
Allison, S.D., Wallenstein, M.D., Bradford, M.A., 2010. Soil-carbon response to warming dependent on microbial physiology. Nat. Geosci. 3, 336–340.
Amadi, C.C., van Rees, K.C.J., Farrell, R.E., 2016. Soil-atmosphere exchange of carbon dioxide, methane and nitrous oxide in shelterbelts compared with adjacent cropped fields. Agric. Ecosyst. Environ. 223, 123–134.
Arnold, J.G., Srinivasan, R., Muttiah, R.S., Williams, J.R., 1998. Large area hydrologic modeling and assessment part I: model development. J. Am. Water Resour. Assoc. 34, 73–89.
Arnold, J.G., Moriasi, D.N., Gassman, P.W., Abbaspour, K.C., White, M.J., Srinivasan, R., Santhi, C., Harmel, R.D., van Griensven, A., van Liew, M.W., Kannan, N., Jha, M.K., 2012. SWAT: model use, calibration, and validation. Am. Soc. Agric. Biol. Eng . 55, 18.
Bethke, C.M., 2007. Geochemical and Biogeochemical Reaction Modeling. Cambridge University Press.
Bethke, C.M., Sanford, R.A., Kirk, M.F., Jin, Q., Flynn, T.M., 2011. The thermodynamic ladder in geomicrobiology. Am. J. Sci. 311, 183–210.
Bhanja, S.N., Wang, J., Shrestha, N.K., Zhang, X., 2019. Microbial kinetics and thermodynamic (MKT) processes for soil organic matter decomposition and dynamic oxidation-reduction potential: model descriptions and applications to soil N_2O emissions. Environ. Pollut. 247, 812–823.
Bond-Lamberty, B., Bailey, V.L., Chen, M., Gough, C.M., Vargas, R., 2018. Globally rising soil heterotrophic respiration over recent decades. Nature 560, 80–83.
Bond-Lamberty, B., Wang, C., Gower, S.T., 2004. A global relationship between the heterotrophic and autotrophic components of soil respiration. Glob. Chang. Biol. 10, 1756–1766.
Bradley, P.M., Chapelle, F.H., 1998. Effect of contaminant concentration on aerobic microbial mineralization of DCE and VC in stream-bed sediments. Environ. Sci. Technol. 32, 553–557.
Bratsch, S.G., 1989. Standard electrode potentials and temperature coefficients in water at 298.15 K. J. Phys. Chem. Ref. Data 18, 1–21.
Brændholt, A., Ibrom, A., Larsen, K.S., Pilegaard, K., 2018. Partitioning of ecosystem respiration in a beech forest. Agric. For. Meteorol. 252, 88–98.
Ciais, P., Sabine, C., Bala, G., Bopp, L., Brovkin, V., Canadell, J., Chhabra, A., DeFries, R., Galloway, J., Heimann, M., Jones, C., 2014. Carbon and other biogeochemical cycles. In: Climate Change 2013: the Physical Science Basis. Contribution of Working Group I to the Fifth Assessment Report of the Intergovernmental Panel on Climate Change. Cambridge University Press, pp. 465–570.
D'Angelo, E.M., Reddy, K.R., 1999. Regulators of heterotrophic microbial potentials in wetland soils. Soil Biol. Biochem. 31, 815–830.
Davidson, E.A., Janssens, I.A., 2006. Temperature sensitivity of soil carbon decomposition and feedbacks to climate change. Nature 440, 165.
Davidson, E.A., Samanta, S., Caramori, S.S., Savage, K., 2012. The Dual Arrhenius and Michaelis–Menten kinetics model for decomposition of soil organic matter at hourly to seasonal time scales. Glob. Chang. Biol. 18, 371–384.
Du, X., Shrestha, N.K., Wang, J., 2019a. Assessing climate change impacts on stream temperature in the Athabasca River Basin using SWAT equilibrium temperature model and its potential impacts on stream ecosystem. Sci. Total Environ. 650, 1872–1881.
Du, X., Shrestha, N.K., Wang, J., 2019b. Integrating organic chemical simulation module into SWAT model with application for PAHs simulation in Athabasca oil sands region, Western Canada. Environ. Model. Softw. https://doi.org/10.1016/j.envsoft.2018.10.011.
Ginn, B., Meile, C., Wilmoth, J., Tang, Y., Thompson, A., 2017. Rapid iron reduction rates are stimulated by high-amplitude redox fluctuations in a tropical forest soil. Environ. Sci. Technol. 51, 3250–3259.
Gliński, J., Stępniewski, W., 1985. Soil Aeration and its Role for Plants. CRC Press, Inc.
Goreau, T.J., Kaplan, W.A., Wofsy, S.C., McElroy, M.B., Valois, F.W., Watson, S.W., 1980. Production of NO_2^- and N_2O by nitrifying bacteria at reduced concentrations of oxygen. Appl. Environ. Microbiol. 40, 526–532.
Grundl, T.J., Stefan, H., Nurmi, J.T., Tratnyek, P.G., 2011. Introduction to aquatic redox chemistry. In: Tratnyek, P.G., Grundl, T.J., Haderlein, S.B. (Eds.), Aquatic Redox Chemistry. American Chemical Society 2011.
Gupta, H.V., Sorooshian, S., Yapo, P.O., 1999. Status of automatic calibration for hydrologic models: comparison with multilevel expert calibration. J. Hydrol. Eng. 4, 135–143.
Hamby, D.M., 1994. A review of techniques for parameter sensitivity analysis of environmental models. Environ. Monit. Assess. 32, 135–154.
Hanson, P.J., Edwards, N.T., Garten, C.T., Andrews, J.A., 2000. Separating root and soil microbial contributions to soil respiration: a review of methods and observations. Biogeochemistry 48, 115–146.
Heimann, M., Reichstein, M., 2008. Terrestrial ecosystem carbon dynamics and climate feedbacks. Nature 451, 289.
Helsel, D.R., Hirsch, R.M., 1992. Statistical Methods in Water Resources, vol. 49 Elsevier.
Hogberg, P., Nordgren, A., Buchmann, N., Taylor, A.F., Ekblad, A., HoÈgberg, M.N., Nyberg, G., Ottosson-LoÈfvenius, M., Read, D.J., 2001. Large-scale forest girdling shows that current photosynthesis drives soil respiration. Nature 411, 789.
Holtan-Hartwig, L., Dörsch, P., Bakken, L.R., 2002. Low temperature control of soil denitrifying communities: kinetics of N_2O production and reduction. Soil Biol. Biochem. 34, 1797–1806.
Jenkinson, D.S., Coleman, K., 2008. The turnover of organic carbon in subsoils. Part 2. Modelling carbon turnover. Eur. J. Soil Sci. 59, 400–413.
Jin, Q., Bethke, C.M., 2005. Predicting the rate of microbial respiration in geochemical environments. Geochem. Cosmochim. Acta 69, 1133–1143.
Jin, Q., Kirk, M.F., 2016. Thermodynamic and kinetic response of microbial reactions to high CO_2. Front. Microbiol. 7, 1696.
Jin, Q., Roden, E.E., Giska, J.R., 2013. Geomicrobial kinetics: extrapolating laboratory studies to natural environments. Geomicrobiol. J. 30, 173–185.
Kirk, G., 2004. The Biogeochemistry of Submerged Soils. John Wiley & Sons.
Lal, R., 2004. Soil carbon sequestration impacts on global climate change and food

security. Science 304, 1623–1627.
Lal, R., 2008. Carbon sequestration. Philos. Trans. R. Soc. Lond. B Biol. Sci. 363, 815–830.
Le Quéré, C., Andrew, R.M., Canadell, J.G., Sitch, S., Korsbakken, J.I., Peters, G.P., Manning, A.C., Boden, T.A., Tans, P.P., Houghton, R.A., Keeling, R.F., 2016. Global carbon budget 2016. 8 Earth System Science Data (Online).
Li, C., Frolking, S., Frolking, T.A., 1992. A model of nitrous oxide evolution from soil driven by rainfall events: 1. Model structure and sensitivity. J. Geophys. Res. Atmos. 97, 9759–9776.
Li, C., Frolking, S., Harriss, R., 1994. Modeling carbon biogeochemistry in agricultural soils. Glob. Biogeochem. Cycles 8, 237–254.
Li, C., Aber, J., Stange, F., Butterbach-Bahl, K., Papen, H., 2000. A process-oriented model of N_2O and NO emissions from forest soils: 1. Model development. J. Geophys. Res.: Atmosphere 105, 4369–4384.
Li, C., Mosier, A., Wassmann, R., Cai, Z., Zheng, X., Huang, Y., Tsuruta, H., Boonjawat, J., Lantin, R., 2004. Modeling greenhouse gas emissions from rice-based production systems: sensitivity and upscaling. Glob. Biogeochem. Cycles 18, GB1043.
Li, C., Frolking, S., Xiao, X.M., Moore, B., Boles, S., Qiu, J.J., Huang, Y., Salas, W., Sass, R., 2005. Modeling impacts of farming management alternatives on CO_2, CH_4, and N_2O emissions: a case study for water management of rice agriculture of China. Glob. Biogeochem. Cycles 19, GB3010.
Li, J., Wang, G., Allison, S., Mayes, M., Luo, Y., 2014. Soil carbon sensitivity to temperature and carbon use efficiency compared across microbial-ecosystem models of varying complexity. Biogeochemistry 119, 67–84.
Louie, S.M., Tilton, R.D., Lowry, G.V., 2013. Effects of molecular weight distribution and chemical properties of natural organic matter on gold nanoparticle aggregation. Environ. Sci. Technol. 47, 4245–4254.
Lovley, D.R., 1987. Organic matter mineralization with the reduction of ferric iron: a review. Geomicrobiol. J. 5, 375–399.
Lovley, D.R., 2008. The microbe electric: conversion of organic matter to electricity. Curr. Opin. Biotechnol. 19, 564–571.
Lovley, D.R., Phillips, E.J., 1986. Organic matter mineralization with reduction of ferric iron in anaerobic sediments. Appl. Environ. Microbiol. 51, 683–689.
Luo, Y., Ahlström, A., Allison, S.D., Batjes, N.H., Brovkin, V., Carvalhais, N., Chappell, A., Ciais, P., Davidson, E.A., Finzi, A., Georgiou, K., 2016. Toward more realistic projections of soil carbon dynamics by Earth system models. Glob. Biogeochem. Cycles 30, 40–56.
Mackay, D., 2001. Multimedia Environmental Models: the Fugacity Approach. CRC press.
Magill, A.H., Aber, J.D., 2000. Dissolved organic carbon and nitrogen relationships in forest litter as affected by nitrogen deposition. Soil Biol. Biochem. 32, 603–613.
Maggi, F., Gu, C., Riley, W.J., Hornberger, G.M., Venterea, R.T., Xu, T., Spycher, N., Steefel, C., Miller, N.L., Oldenburg, C.M., 2008. A mechanistic treatment of the dominant soil nitrogen cycling processes: Model development, testing, and application. J. Geophys. Res.: Biogeosci. 113 (G2). https://doi.org/10.1029/2007JG000578.
Manzoni, S., Jackson, R.B., Trofymow, J.A., Porporato, A., 2008. The global stoichiometry of litter nitrogen mineralization. Science 321, 684–686.
McBride, M.B., 1994. Environmental Chemistry of Soils. Oxford University press.
Meng, Y., Zhou, L., He, S., Lu, C., Wu, G., Ye, W., Ji, P., 2018. A heavy metal module coupled with the SWAT model and its preliminary application in a mine-impacted watershed in China. Sci. Total Environ. 613, 1207–1219.
Mitchard, E.T., 2018. The tropical forest carbon cycle and climate change. Nature 559, 527.
Moriasi, D.N., Arnold, J.G., van Liew, M.W., Bingner, R.L., Harmel, R.D., Veith, T.L., 2007. Model evaluation guidelines for systematic quantification of accuracy in watershed simulations. Transactions of the ASABE 50, 885–900.
Nash, J.E., Sutcliffe, J.V., 1970. River flow forecasting through conceptual models part I—a discussion of principles. J. Hydrol. 10, 282–290.
Neitsch, S.L., Arnold, J.G., Kiniry, J.R., Williams, J.R., 2011. Soil and Water Assessment Tool Theoretical Documentation Version 2009. Texas Water Resources Institute.
Noll, M., Matthies, D., Frenzel, P., Derakshani, M., Liesack, W., 2005. Succession of bacterial community structure and diversity in a paddy soil oxygen gradient. Environ. Microbiol. 7, 382–395.
Pallud, C., van Cappellen, P., 2006. Kinetics of microbial sulfate reduction in estuarine sediments. Geochem. Cosmochim. Acta 70, 1148–1162.
Parnas, H., 1975. Model for decomposition of organic material by microorganisms. Soil Biol. Biochem. 7, 161–169.
Parton, W.J., 1996. The CENTURY model. In: Powlson, D.S., Smith, P., Smith, J.U. (Eds.), Evaluation of Soil Organic Matter Models. Springer, Berlin.
Parton, W.J., Schimel, D.S., Cole, C.V., Ojima, D.S., 1987. Analysis of factors controlling soil organic matter levels in Great Plains Grasslands 1. Soil Sci. Soc. Am. J. 51, 1173–1179.
Parton, W.J., Hartman, M., Ojima, D., Schimel, D., 1998. DAYCENT and its land surface submodel: description and testing. Glob. Planet. Chang. 19, 35–48.
Patrick, W.H., Jugsujinda, A., 1992. Sequential reduction and oxidation of inorganic nitrogen, manganese, and iron in flooded soil. Soil Sci. Soc. Am. J. 56, 1071–1073.
Peters, V., Conrad, R., 1996. Sequential reduction processes and initiation of CH4 production upon flooding of oxic upland soils. Soil Biol. Biochem. 28, 371–382.
Pidello, A., 2003. Environmental redox potential and redox capacity concepts using a simple polarographic experiment. J. Chem. Educ. 80, 68.
Postma, D., Jakobsen, R., 1996. Redox zonation: equilibrium constraints on the Fe (III)/SO4-reduction interface. Geochem. Cosmochim. Acta 60, 3169–3175.
Quin, P., Joseph, S., Husson, O., Donne, S., Mitchell, D., Munroe, P., Phelan, D., Cowie, A., van Zwieten, L., 2015. Lowering N 2 O emissions from soils using eucalypt biochar: the importance of redox reactions. Sci. Rep. 5, 6773.
Reddy, K.R., DeLaune, R.D., 2008. Biogeochemistry of Wetlands: Science and Applications. CRC press.
Sander, R., 2015. Compilation of Henry's law constants (version 4.0) for water as solvent. Atmos. Chem. Phys. 15.
Shrestha, N.K., Wang, J., 2018. Current and future hot-spots and hot-moments of nitrous oxide emission in a cold climate river basin. Environ. Pollut. 239, 648–660.
Shrestha, N.K., Du, X., Wang, J., 2017. Assessing climate change impacts on fresh water resources of the Athabasca River Basin, Canada. Sci. Total Environ. 601, 425–440.
Shrestha, N.K., Thomas, B.W., Du, X., Hao, X., Wang, J., 2018. Modeling nitrous oxide emissions from rough fescue grassland soils subjected to long-term grazing of different intensities using the Soil and Water Assessment Tool (SWAT). Environ. Sci. Pollut. Res. 25 (27), 27362–27377.
Srinivasan, R., Zhang, X., Arnold, J., 2010. SWAT ungauged: hydrological budget and crop yield predictions in the Upper Mississippi River Basin. Trans. ASABE 53, 1533–1546.
Stumm, W., Morgan, J.J., 1996. Aquatic Chemistry: Chemical Equilibria and Rates in Natural Waters. Wiley.
Tan, K.H., 2010. Principles of Soil Chemistry. CRC press, pp. 362.
Todd-Brown, K.E.O., Randerson, J.T., Hopkins, F., Arora, V., Hajima, T., Jones, C., Shevliakova, E., Tjiputra, J., Volodin, E., Wu, T., Zhang, Q., 2014. Changes in soil organic carbon storage predicted by Earth system models during the 21st century. Biogeosciences 11, 2341–2356.
Tukey, J.W., 1977. Exploratory Data Analysis, vol. 2 Addison-Wesley Publishing Company.
van Bodegom, P.M., Scholten, J.C., 2001. Microbial processes of CH4 production in a rice paddy soil: model and experimental validation. Geochem. Cosmochim. Acta 65, 2055–2066.
van Bodegom, P.M., Stams, A.J.M., 1999. Effects of alternative electron acceptors and temperature on methanogenesis in rice paddy soils. Chemosphere 39, 167–182.
Van't Hoff, J.H., Lehfeldt, R.A., 1899. Lectures on Theoretical and Physical Chemistry.
Wagena, M.B., Bock, E.M., Sommerlot, A.R., Fuka, D.R., Easton, Z.M., 2017. Development of a nitrous oxide routine for the SWAT model to assess greenhouse gas emissions from agroecosystems. Environ. Model. Softw 89, 131e143.
Wang, G.S., Post, W.M., Mayes, M.A., 2013. Development of microbial-enzyme-mediated decomposition model parameters through steady-state and dynamic analyses. Ecol. Appl. 23, 255–272.
Wieder, W.R., Bonan, G.B., Allison, S.D., 2013. Global soil carbon projections are improved by modelling microbial processes. Nat. Clim. Change 3, 909.
Wieder, W.R., Cleveland, C.C., Smith, W.K., Todd-Brown, K., 2015. Future productivity and carbon storage limited by terrestrial nutrient availability. Nat. Geosci. 8, 441.
Yadav, D., Wang, J., 2017. Modelling carbon dioxide emissions from agricultural soils in Canada. Environ. Pollut. 230, 1040–1049.
Yan, Z., Bond-Lamberty, B., Todd-Brown, K.E., Bailey, V.L., Li, S., Liu, C., Liu, C., 2018. A moisture function of soil heterotrophic respiration that incorporates microscale processes. Nat. Commun. 9, 2562.
Yang, Q., Zhang, X., Abraha, M., Del Grosso, S., Robertson, G.P., Chen, J., 2017. Enhancing the soil and water assessment tool model for simulating N2O emissions of three agricultural systems. Ecosyst. Health Sustain 3 (2), 1–13.
Zhang, X., Izaurralde, R.C., Arnold, J.G., Williams, J.R., Srinivasan, R., 2013. Modifying the soil and water assessment tool to simulate cropland carbon flux: model development and initial evaluation. Sci. Total Environ. 463, 810–822.